Analysis of exocytotic events recorded by amperometry

Eugene V Mosharov[1] & David Sulzer[1–3]

Amperometry is widely used to study exocytosis of neurotransmitters and hormones in various cell types. Analysis of the shape of the amperometric spikes that originate from the oxidation of monoamine molecules released during the fusion of individual secretory vesicles provides information about molecular steps involved in stimulation-dependent transmitter release. Here we present an overview of the methodology of amperometric signal processing, including (i) amperometric signal acquisition and filtering, (ii) detection of exocytotic events and determining spike shape characteristics, and (iii) data manipulation and statistical analysis. The purpose of this review is to provide practical guidelines for performing amperometric recordings of exocytotic activity and interpreting the results based on shape characteristics of individual release events.

The introduction of electrochemical detection of transmitters[1] and the development of the carbon fiber microelectrode[2] have provided a means to directly measure vesicular release of neurotransmitters and hormones from presynaptic neurons and other secretory cells. After the initial work by Wightman's group on chromaffin cells[3,4], several laboratories adapted amperometry to study exocytosis of large dense core vesicles (LDCV) and small synaptic vesicles (SSV) containing various chemical messengers, including catecholamines (pheochromocytoma (PC12) cells[5], midbrain dopaminergic neurons[6], sympathetic ganglion neurons[7], snail neurons[8]), serotonin (mast cells[9], leech neurons[10]) and peptides (pancreatic β-cells[11], pituitary melanotrophs[12]). These studies have provided valuable information about the operation of vesicle fusion machinery, shaping our present understanding of the mechanisms underlying secretory neurotransmission.

During amperometric recordings, a carbon fiber electrode held at a positive potential is placed against the surface of a secretory cell (see refs. 13 and 14 for electrode fabrication techniques). Exocytotic activity is observed as amperometric 'spikes'—electrochemical current caused by the transfer of electrons after monoamine oxidation. The sensitivity of amperometry permits quantification of the transmitter molecules released from individual vesicles, providing information about intracellular transmitter homeostasis (synthesis, degradation, reuptake and other processes), whereas measurements of spike frequency provide information about the vesicle release probability. Furthermore, the excellent temporal resolution of amperometry allows observation of the real-time kinetics of monoamine release during exocytosis. In particular, the properties of the initial 'fusion pores', narrow channels connecting vesicle lumen with the external medium, can be studied. Additionally, simultaneous amperometric detection of monoamine release and measurements of changes in plasma membrane capacitance and pore conductance during the fusion of individual vesicles comprise one of the most advanced systems for studying various modes of exocytotic release to date[15]. Here we review algorithms used for acquisition, detection and analysis of amperometric events (Fig. 1) with emphasis on procedures that provide consistent determination of spike parameters on recordings with different sampling rates, signal-to-noise levels, spike durations and surrounding signal.

[1]Departments of Neurology and [2]Psychiatry, Black Building 305, 650 W 168th Street, Columbia University, New York, New York 10032, USA. [3]Department of Neuroscience, New York State Psychiatric Institute, 722 W 168th Street, New York, New York 10032, USA. Correspondence should be addressed to E.V.M. (em706@columbia.edu).

PUBLISHED ONLINE 23 AUGUST 2005; DOI:10.1038/NMETH782

DISSECTING THE AMPEROMETRIC SIGNAL

Initiation of fusion

Fusion of a vesicle with the plasma membrane, which has been studied by amperometry primarily in LDCV cells, is thought to begin with the soluble *N*-ethylmaleimide–sensitive factor attachment protein receptor (SNARE) complex–coordinated formation of the fusion pore (reviewed in refs. 16–18). Amperometrically, the flux of monoamines through the pore is resolved as a prespike foot (PSF), a small current step that precedes many spikes, first reported by Chow and colleagues[19,20]. Work by several groups showed that pharmacological and genetic manipulations of various members of the fusion machinery can modulate both monoamine flux through the fusion pore and pore stability. These parameters are estimated from PSF amplitude and duration, respectively (reviewed in refs. 18 and 21). Simultaneous amperometric and capacitance measurements demonstrate that the current during the foot originates from the release of free vesicular monoamine[9,22], whereas the majority of transmitter is stored in a complex with a polyelectrolyte matrix (reviewed in ref. 23). PSF current depends on several factors, including fusion pore geometry, free vesicular concentration of the transmitter[9,22] and possibly the ability of counterions to dissipate the electrochemical gradient created within the catecholamine-containing vesicles[24]. Notably, the fraction of spikes with a foot and the proportion of total vesicular transmitter content released during PSF depend on vesicle size[9,25,26], implying that physical properties of the fusing membranes (curvature, rigidity, and others) and the proportion of vesicular volume occupied by the matrix may also regulate fusion pore kinetics.

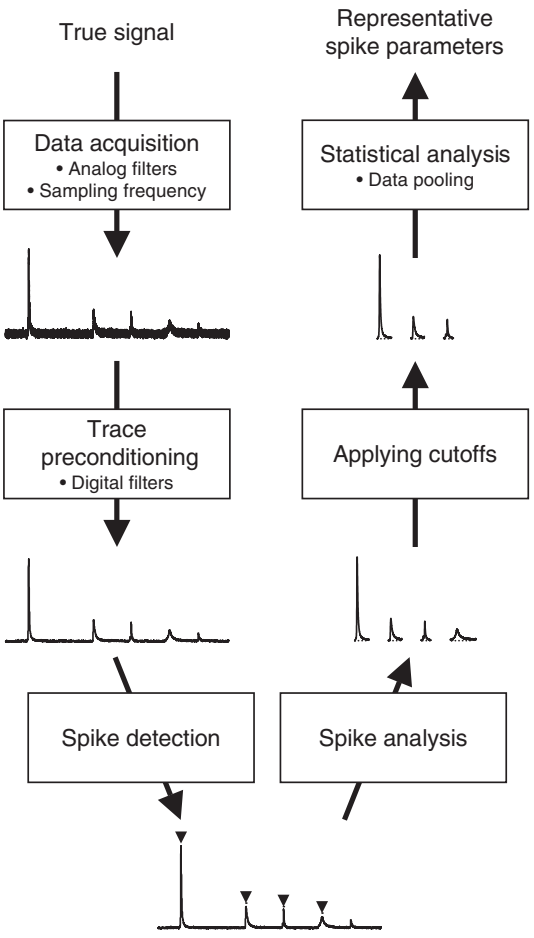

Different modes of exocytotic fusion

The initial fusion pore opening is followed by an exchange of ions and water between the extracellular medium and vesicular lumen, and swelling of the intravesicular polyelectrolyte matrix[27–29]. The interplay between the increasing internal swelling pressure and the edge energy of the pore, which are affected by vesicular and cellular membrane viscosities and tension, has been suggested to contribute to fusion pore instability[23,30]. Consequently, the thermodynamically unfavorable fusion pore conformation progresses into distinct modes of transmitter release that can be distinguished by combined amperometric and capacitance measurements.

During full fusion, the predominant mode of exocytosis for LDCV-releasing cells, the fusion pore expands abruptly, leading to a complete collapse of the vesicle into the plasma membrane and a massive release of stored monoamines. Full fusion is observed as a capacitance step and an amperometric spike with characteristic steep rising and slow decay kinetics[9,13,19]. Alternatively, the pore can reclose to produce a stand-alone foot, which is distinguished by a capacitance flicker. Although the amperometric signal accompanying such events has slow kinetics governed by monoamine extrusion through a narrow fusion pore, nearly the entire vesicle content can be exocytosed during stand-alone feet[9,20,22]. Yet another distinct mode of exocytosis occurs when pore closure is preceded by an abrupt and brief fusion pore expansion, allowing fast monoamine release amperometrically indistinguishable from that during the full fusion, an event termed 'kiss-and-run' exocytosis[31]. It is thought that vesicle membrane retrieval during kiss-and-run events is mediated by rapid endocytosis via non–clathrin-mediated mechanism (reviewed in refs. 32 and 33).

It is still a matter of debate whether the fusion pore size restricts the release of transmitter during the fast rising phase of the spikes, and whether fusion pore closure can regulate the quantal size of monoamine release during LDCV exocytosis. Although several studies support this possibility based on the effects of second messengers and fusion pore protein modifications on the shape of amperometric spikes (reviewed in ref. 18), measurements of the expanding pore conductance during the upstroke of amperometric current indicate that its size might be too large to limit monoamine diffusion from the vesicle[34]. Alternative explanations for these data may include the effects on transmitter loading into the vesicles[35] or its dissociation from the matrix[23]; experiments combining amperometric and capacitance measurements are required to resolve this controversy. In contrast to LDCV exocytotic release, amperometric studies of exocytosis from midbrain neurons suggest that PKC-dependent flickering of the fusion pore between open and closed conformations may indeed regulate the quantal size of neurotransmitter release from SSVs by several fold, although the mechanism of such regulation remains unknown[36].

After fusion

During the final, postfusion phase of an exocytotic event, diffusion of transmitter molecules to the electrode affects the shape of

Figure 1 | An overview of amperometric data acquisition and analysis. The original 'true' amperometric signal is ultimately represented by spike characteristics pooled and analyzed from several recordings. During the processing of individual traces, each analytical step may introduce some signal distortion, depending on the internal characteristics of the recording (signal frequencies, noise level and others) and on user-defined parameters of the analysis (digital filters, detection thresholds, cutoffs and others).

amperometric spikes similarly to a low-pass filter—the spikes become smaller and wider as the diffusional distance increases[13,37]. Additionally, the apparent quantal size of such events may decrease because only a portion of transmitter molecules reaches the detection electrode[14,38]. Even when exocytotic activity is recorded with the electrode positioned to minimize diffusional distance, events from LDCV-containing cells are still wider than predicted for a process controlled only by diffusion[23]. Considerable evidence suggests that the kinetics of transmitter dissociation from and diffusion through the expanding polyelectrolyte matrix are the rate limiting steps determining the shape of the amperometric spike's 'tail', a slow decay of current to background levels[39]. Notably, whereas the latter can be fit by a single-exponent in some amperometric events[4,40], other spikes have decay kinetics that require double-exponential fit functions[41]. Further experiments are necessary to establish the determinants of these processes including possible involvement of SNARE proteins[41].

Additional factors that affect various shape characteristics of amperometric events include drug treatments, stimulation frequency, intra- and extracellular [Ca^{2+}], vesicular and external pH, temperature and many others (reviewed in refs. 13, 35 and 39). Although analysis of each spike feature contributes to a comprehensive understanding of the functioning of the vesicle cycle and fusion machinery, there has been no consensus regarding certain aspects of the analysis, complicating the comparison of data between various sources.

BOX 1 RECOMMENDATION: FILTERING TECHNIQUES

Choosing a filter for a particular type of recording to achieve maximal noise reduction without significant signal distortion is a complicated task[58]. Borges' group developed an alternative to the single 'optimal' filter, which includes using different filters depending on the signal frequencies present in each trace segment[59]. An alternative approach involves filtering the nondifferentiated trace in two steps. A filter with a corner frequency higher than the frequency of the signal is used to reduce the noise for spike analysis (arrow 1), whereas a separate coarser filter with a corner frequency lower than the frequency of the signal is used to enhance the signal-to-noise ratio (arrow 2; see **Supplementary Methods** for guidelines on choosing the cutoffs). This method can be used for spike detection using either nondifferentiated (#) or differentiated (##) traces. The advantage of this design is that although additional current filtering improves the sensitivity of spike detection, the trace that is ultimately analyzed (*) is filtered only once, making it easier to account for possible signal distortion.

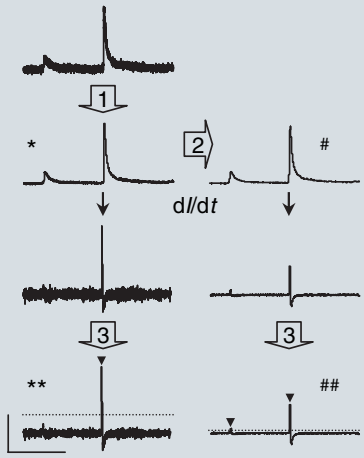

Three low-pass Gaussian filters are: 1–600 Hz (F_{c1}), 2–150 Hz (F_{c2}), and 3–300 Hz (F_{c3}). Arrowheads in the bottom panels indicate spikes that exceed 5 × $SD_{dI/dt}$ (dotted lines). Scale bars, 20 pA for the current, 10 pA/ms for d*I*/d*t* and 100 ms for the timescale.

If dI/dt is used, a third digital filter is used to counter the decrease of signal-to-noise during differentiation (arrow 3), and a lightly-filtered copy of the differential is generated (**) to be used when analyzing the spike rising phase (see **Box 2**).

ACQUISITION AND ANALYSIS OF AMPEROMETRIC SPIKES

Data acquisition and filtering

A typical electrophysiology setup comprises an amplifier to control the voltage and measure the current at the electrode, and an analog-to-digital converter (ADC) to transform the signal to a digital format. The design of the setup places a hardware limit on its frequency response so that its current output can be considered a filtered version of the 'true' signal. The two major parameters that determine the degree of signal distortion during data acquisition are the corner frequency (cutoff) of an analog filter of the amplifier and the sampling rate of the analog-to-digital converter. To avoid aliasing and to accurately reconstitute the waveform, the sampling rate should be at least twice the cutoff frequency of the filter and at least ten times the highest frequency component of the signal of interest[42]. The latter consideration is especially stringent during recordings from SSV cells, for which the data should be sampled at rates of at least 100 kHz to monitor amperometric spikes with an average duration of 100 μs[35].

Amperometric traces stored on the computer are commonly digitally filtered to enhance the sensitivity of spike detection[42]. Conversely, to preserve the signal of interest, overfiltering should be avoided as it distorts spike shapes by reducing amplitude and increasing duration. The choice of appropriate filters becomes especially critical when analyzing the slope of the spike rising phase, as this parameter, representing the highest frequency present in the signal, is most sensitive to low-pass filtering applied to the data. Different laboratories use filters with response characteristics (type, cutoff, steepness, group delay and others) intended to provide the most consistent representation of the 'true' signal. The two most often used filters are low-pass filters (Bessel, Gaussian, rolling-off and others) that attenuate high-frequency 'white' noise, and notch filters that eliminate line frequency noise at 50/60 Hz. Preference should be given to filters that are better-suited for time domain analysis and therefore have constant group delay and do not produce rippling of the current (Gibbs phenomenon). Additionally, a combination of filters with different cutoffs often produces better spike detection efficiency and signal preservation (Box 1).

Detection of amperometric spikes

Two approaches are used to detect spikes in amperometric traces—a spike is identified when either the current (I) or its time derivative (dI/dt) exceeds a user-defined threshold (Fig. 2). As the threshold is usually a multiple of the standard deviation of the noise (SD_I) or its derivative ($SD_{dI/dt}$) calculated on a spike-free segment of a trace, the number of detected spikes depends on the noise level, which may vary several fold between the recordings. An alternative to only ana-

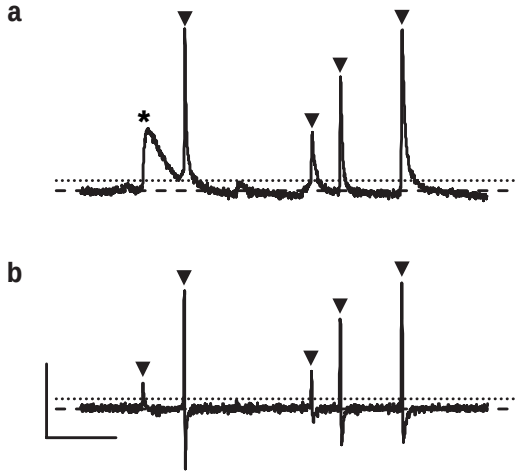

Figure 2 | Detection of amperometric events. (**a**) Spike detection using nondifferentiated current. Because of a slight downward background drift, spike baselines and thus all other parameters will be calculated improperly, unless the background current is reestablished before each spike. Additionally, the first of the two overlapping spikes (*) will be identified as the foot of the second spike. (**b**) Spike detection using time derivative of the current. Dashed lines represent background current before the first spike in **a** and zero line in **b**. Arrowheads indicate spikes that exceed $5 \times SD_I$ or $5 \times SD_{dI/dt}$ (dotted lines). Scale bars, 50 pA (**a**), 40 pA/ms (**b**) and 100 ms for the timescale.

lyzing traces that have the same noise level, which can be experimentally challenging, is to use an amplitude cutoff function, which makes detection procedures less dependent on the noise present in individual recordings (see below).

Detection protocols that identify amperometric spikes using SD_I threshold were originally designed in the Wightman laboratory[4,43] and have been used by many researchers to analyze amperometric traces from various cell types. For recordings with a stable baseline or during manual spike detection, this protocol is somewhat more reliable as it provides more straightforward definitions of spike beginning and end (Supplementary Methods online). It may, however, become unstable during automated spike analysis in the presence of low-frequency noise introduced by application of drugs or secretagogues, caged Ca^{2+} pulses or other baseline drifts (Fig. 2a). Commonly used methods to counter this include trace conditioning either by high-pass filtering[4] or by subtracting a 'secretion envelope' generated by recording the current under the same experimental conditions but in the absence of exocytotic activity[44]. These methods, however, are not very precise in correcting the baseline, which still needs to be manually readjusted. Additionally, high-pass filtering may affect spike feet, which are often in the same frequency range as the noise.

In contrast, because differentiation discriminates against low frequencies, an approach that uses a $SD_{dI/dt}$ threshold is more convenient for computerized spike detection as dI/dt is stably positioned around zero[45] (Fig. 2b). Two problems arise when dI/dt is used for event detection. First, in a typical amperometric trace, differentiation decreases the signal-to-noise ratio thereby demanding additional filtering of the dI/dt (Box 1). Second, this method may perform poorly when determining the baseline of spikes that have PSF with very long steady-state signals (see next).

Calculation of spike parameters

As each consecutive step during the analysis of individual amperometric events uses spike parameters determined in the preceding ones (Fig. 3), the first step, establishing spike baseline (Fig. 3a), can be considered as most critical because its outcome affects all other spike characteristics. It is, however, rather challenging to design an entirely user-independent algorithm that finds beginnings and ends for spikes of all possible shapes and arrangements in the trace (baseline drifts, spike overlaps and others). Additionally, the presence of high-frequency noise complicates the search for the timepoint when the transmitter concentration declines to the initial levels. Although some procedures can improve proper baseline positioning (Supplementary Fig. 1 online and Supplementary Methods), visual trace examination and baseline readjustment are often necessary.

After the baseline and time at spike maximum (T_{max}) are determined, basic peak characteristics—amplitude (I_{max}), half width ($t_{1/2}$) and charge (Q)—can be calculated by straightforward proce-

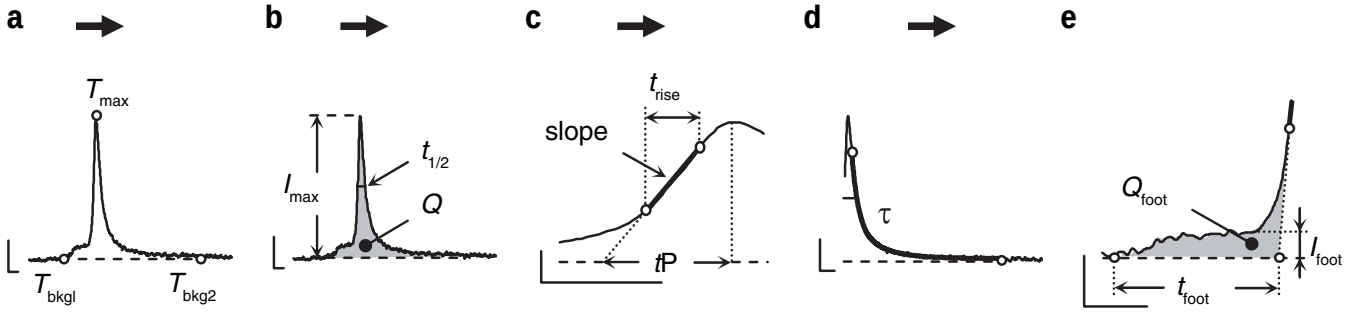

Figure 3 | Calculation of spike parameters. (**a**) Establishing spike baseline (dashed line). T_{max} is time at spike maximum; T_{bkg1} and T_{bkg2} are spike beginning and end, respectively (see **Supplementary Methods** for algorithms). (**b**) Spike amplitude, I_{max} (A), is measured between the current at T_{max} and the baseline current under the spike maximum. Spike width, $t_{1/2}$ (s), is evaluated at 50% of I_{max}. The amount of transmitter released during an exocytotic event, Q (A × s, Coulomb; C), is estimated from spike area above the baseline (gray). For catecholamine release, the number of transmitter molecules, N, is calculated as $N = Q \div (n \times F) = Q \times 3.121 \times 10^6$ (molecules/pC), where F is Faraday's constant (96,480 C/mole) and n is the number of electrons donated by each oxidized molecule, which for catechols equals two[1,57] (see **Supplementary Methods**). (**c**) Rising phase parameters, slope (A/s), risetime (t_{rise}, s), and time to peak (tP, s), are calculated using linear fit of the current between two points on the ascending segment of the spike (**Box 2**). (**d**) Spike falling phase is represented by the time constants of single- or double-exponential fits of the current between 75% of I_{max} and T_{bkg2}. (**e**) PSF parameters, I_{foot}, t_{foot} and Q_{foot}, are calculated on the spike segment that precedes the extrapolated linear fit of the rising phase (**Box 3**). Scale bars, 20 pA and 2.5 ms.

dures that, to our knowledge, have not significantly changed since the introduction of the first multipass algorithms for spike detection and analysis[43,46] (Fig. 3b). Unfortunately, as discussed below, there has been no consensus concerning the approaches to analyze other spike features. We attempt to provide recommendations on how to analyze these troublesome spike characteristics with the aim of simplifying comparison of data from different laboratories (Boxes 2 and 3).

Risetime (t_{rise}) and slope of the rising phase are derived from the linear fit of the current between two points on the ascending segment of the spike (Fig. 3c and Box 2). The upper point is usually at less than 90% of I_{max} to prevent including the topmost portion of the spike, which is often flattened by filtering. For the lower point, levels from 20% to 50% of I_{max} have been used to avoid including the foot[13,40], the size of which is variable relative to the main spike. Time to peak (*t*P), the duration from the beginning of spike excluding the foot to T_{max}[45], is essentially a t_{rise} from zero to 100% of I_{max}. Although it is simple to normalize t_{rise} to some arbitrary, commonly used value (for example, 25–75% of I_{max}), no such standardization currently exists.

As mentioned, the falling phases of amperometric events from LDCV recordings are fitted with either single- or double-exponential functions (Fig. 3d). Using the ratio of χ^2 values for the fits of the current between 75% of I_{max} and spike end as a cutoff (see Supplementary Table 1 online), we estimated that 45% of the spikes from chromaffin cell recordings have falling phases that are better-fit with a double-exponential function, similar to results by Wang and coauthors on PC12 cells[41]. Notably, amperometric spikes with single-exponential falling phases were on average considerably shorter, wider and had less charge and longer risetimes (Fig. 4). Taken together, these changes are characteristic of release events that originate far away from the electrode and undergo 'diffusional filtering', similar to the subpopulation of spikes that have longer t_{rise} values[13]. Supporting this idea, the incidence of observing a foot was higher for spikes that had shorter t_{rise} or double-exponential falling phases (Supplementary Table 1). Nevertheless, spikes with and without the PSF had similar durations and risetimes, arguing against a possibility that the foot can be observed exclusively within the subpopulation of release events occurring closest to the electrode (Supplementary Fig. 2 online).

PSF parameters

The variability of sizes and shapes of PSF complicates the design of uniform algorithms that identify the parameters of the foot—amplitude (I_{foot}), duration (t_{foot}) and charge (Q_{foot}) (Fig. 3e and Box 3). Although 50–80% of the amperometric events have some kind of pre-spike transitional current that precedes the fast upstroke of the spike[13,30] (Supplementary Fig. 2), sometimes this current reaches a plateau representing an equilibrium between the rates of monoamine release from the vesicle and consumption by the electrode. Whereas I_{foot} can be determined with higher accuracy on feet with steady states, the interpretation of this parameter itself is not trivial.

Foot current is proportional to the flux *j* of catecholamines through a cylindrical fusion pore[37]:

$$I_{foot} \propto j = \frac{\pi \times R_{pore}^2}{L_{pore}} \times (C_v - C_{ex}) \times D$$

where R_{pore} is the radius and L_{pore} is the length of the pore, C_v and C_{ex} are the concentration of transmitter inside and outside of the vesicle, and *D* is the diffusion coefficient. It has been demonstrated that for PSF recorded from individual cells, I_{foot} is linearly proportional to fusion pore conductance[9,22], implying that geometric parameters of individual pores control the flux of the transmitter,

BOX 2 RECOMMENDATION: SPIKE RISING PHASE PARAMETERS

A robust method of finding the middle of the linear segment of the rising phase uses the maximum of the differentiated trace, $T(dI/dt)_{max}$. Two points used to perform the linear fit and to calculate rising phase slope (filled circles) are found as (current at $T(dI/dt)_{max}$) ± (1/2 of ΔI between currents at T_{max} and $T(dI/dt)_{max}$). For a spike without PSF, these points correspond to 25% and 75% of I_{max}. The interception of the extrapolated linear fit to spike baseline (solid line) is used to find the end of the spike foot (**Box 3**) and to derive t_{rise}. The latter is estimated as percentage of *t*P, which is calculated between the extrapolated fit interception and T_{max}. As t_{rise} becomes independent of the relative PSF height and the length of the linear segment, its value can be recalculated for any arbitrary percentage of spike rising phase, simplifying data comparison between different experimental groups or cell types.

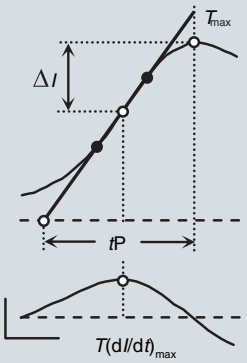

Amperometric current (top) and its time derivative (bottom); dashed lines represent the spike baseline on the current trace or zero line on the differential trace. Scale bars, 20 pA for the current, 40 pA/ms for d*I*/d*t* and 1 ms for the timescale.

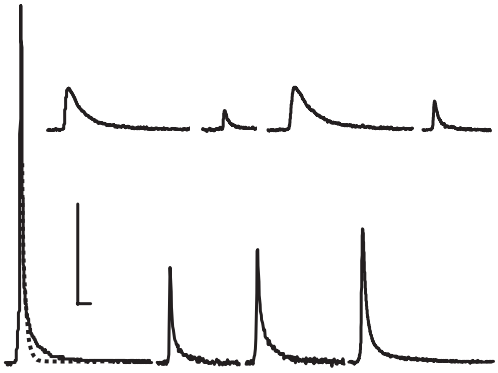

Figure 4 | Spikes with different falling phase kinetics. Examples of spikes with falling phases that were better fit with single- (upper row) or double-exponential (lower row) decay functions. All amperometric events belong to the same experimental trace. Dotted line on the leftmost spike represents a single-exponential fit of current between 75% I_{max} and T_{bkg2}. Scale bars, 50 pA and 10 ms.

BOX 3 RECOMMENDATION: FOOT PARAMETERS

In the original method described by Chow and colleagues[13,19], the beginning of PSF is defined as the time when the amperometric signal exceeds the baseline noise by $2 \times SD_I$ (**a**). This, however, creates a problem that fewer PSFs with smaller durations are found on traces with higher noise. We therefore use the beginning of the spike as PSF start, whereas a multiple of SD_I and minimal I_{foot} are used as cutoffs to remove feet that are buried in the noise, which is similar to using an I_{max} cutoff for spike detection. Foot end is found by extrapolating the linear fit of the rising slope (dotted straight lines) to the baseline of the spike[13] (point 1 in **a**; see also **Box 2**). Alternatively, it can be found at the maximum of the second derivative of the current[25], although this is only applicable for spikes with high signal-to-noise ratio. Foot duration, t_{foot}, is measured between T_{bkg1} and PSF end, and foot charge, Q_{foot}, is the area of the region that precedes the linear rising phase of the spike. Foot current can be determined differently depending on the PSF shape. If all feet are analyzed, the amplitude of PSFs that do not reach steady state cannot be measured directly and therefore is resolved as an average current within t_{foot} (**b**, horizontal solid line). If only PSFs with steady states are analyzed (see **Supplementary Fig. 1** for the methodology of finding the steady state), I_{foot} can be determined with better precision using an averaged current on the PSF plateau (**c**) or an exponential fit of the trace from T_{bkg1} to the end of the foot[22] (**a**, dotted curved line).

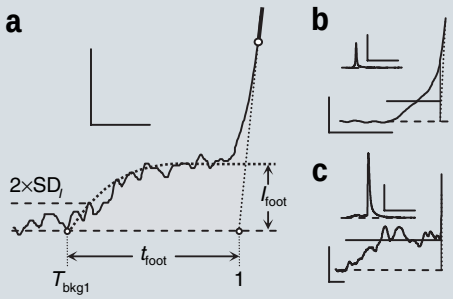

Characterization of foot parameters (a) and examples of PSF without (b) and with (c) detectable steady states. Scale bars, 10 pA and 5 ms for the panels, and 100 pA and 50 ms for the insets in b and c.

whereas monoamine concentration in the vesicles of a given cell is constant. This relationship, however, seemed not to hold when PSF characteristics from several cells were analyzed, as transmitter flux through the pores of similar sizes may vary several fold from cell to cell[9,22]. In agreement with these findings, we observed a skewedness in the distributions of pooled $(I_{foot})^{1/2}$ values (Supplementary Fig. 2) suggesting that R_{pore} is not the only variable that determines the flux of molecules through the pore. Foot current thus appears to be a function of at least two parameters—fusion pore conductance and free vesicular monoamine concentration—and the contribution of each variable is unknown.

DATA MANIPULATION AND ANALYSIS

Rejection of spikes using cutoff criteria

The threshold for any cutoff criterion should be carefully evaluated, particularly if the cutoff parameter itself is influenced by treatments used in a study. For example, because many pharmacological and genetic manipulations affect t_{rise} of the spikes, using it as a cutoff in such studies may bias the populations of spike characteristics in some experimental groups. Hence the distribution of spike characteristics before and after a cutoff is introduced should be examined to check for possible population distortions.

Guidelines for using some common cutoffs are listed in Table 1. Among them, I_{max} is probably the most popular—to our knowledge, most researchers disregard LDCV amperometric events with $I_{max} < 3$–5 pA. First, this cutoff eliminates very small spikes that are buried in the noise and are difficult to analyze reliably. Second, when the I_{max} cutoff is higher than the detection threshold, spike detection becomes less dependent on the level of noise present in each individual recording—small spikes that will be detected on recordings with lower noise will be rejected during the analysis anyway. Similarly, it simplifies the comparison of data from studies that utilize different detection or filtering protocols by decreasing the number of hard-to-detect events that would be found by a more sensitive method. Clearly, using I_{max} as a cutoff requires some preliminary analysis of the noise present in all experimental traces.

As discussed, spike parameters can be distorted by 'diffusional filtering', and thus maximal $t_{1/2}$ or t_{rise} are sometimes used as cutoffs to eliminate 'slow' spikes[13,22] (Supplementary Table 1). Our data also suggest that the shape of the spike falling phase might be indicative of the proximity of the release site to the electrode surface, although alternative explanations, such as the presence of different vesicle populations cannot be excluded. Surprisingly, the slope of the spike rising

Table 1 | Guidelines for applying cutoffs

Cutoff	When appropriate	When inappropriate
Minimal I_{max}, I_{foot}	To discard events that are difficult to analyze. (Analysis becomes less dependent on the noise of individual recordings.)	When the cutoff severely distorts parameter distributions.
Maximal t_{rise}, $t_{1/2}$	To discard events that originate far away from the electrode.	When the cutoff severely distorts parameter distributions.
Discard overlaps	To restrict the analysis to well-resolved spikes.	When analyzing release probability or when the occurrence of overlaps is significantly higher than the probability of random overlaps.

phase, the parameter most sensitive to diffusional distortion, has never been used as a cutoff.

Another cutoff sometimes used during PSF analysis is intended to only consider the feet originating from transmitter release via a restricting fusion pore. The duration of 'native' PSF that are present even during instantaneous transmitter release[13] are estimated as $0.33 \times t_{rise}(50–90\%)$. On chromaffin cell recordings, discarding these 'native' feet has only a minor effect on the averaged spike and PSF values (Supplementary Fig. 2).

Finally, the quality of the rising and falling phases fits can be used as a marker for the validity of a spike's shape[4,13]. For example, amperometric events that have zero correlation with an exponentially modified Gaussian[40,47] or have negative values for any parameter are obviously deleted.

Analysis of overlapping spikes

There have been no established guidelines regarding the exclusion of overlaps from the analysis. Although it seems reasonable to eliminate the overlaps when studying the fine kinetics of amperometric events (PSF, falling phase)[13], other spike parameters ($t_{1/2}$, I_{max}, Q, t_{rise}) can often be approximated within 15% accuracy even in extreme overlap cases (Supplementary Fig. 3 online). There may also be additional reasons against discarding overlapping spikes that are dictated by the aims of a study. Deleting overlaps may substantially reduce the subpopulation of wider spikes, which have higher probability of overlap. Moreover, as pointed out by Sorensen and colleagues[48], a similar problem arises when analyzing two spike populations from cells that have different release probabilities, as a higher release probability leads to an increased incidence of random overlap. Finally, some overlaps are not random but are due to clustered vesicles, compound exocytosis[49,50] or flickering of the fusion pore of neuronal vesicles[36], and thus have important information that would be lost.

The probability of random overlap after stimulated secretion can be evaluated as $P = 1 - e^{(-t/\tau)}$, where t is the average $t_{1/2}$ of amperometric spikes and τ is the time constant of the exponential fit of interspike interval distribution[35]. One often desirable way of reducing the number of random spike overlaps is to choose experimental conditions that induce fewer exocytotic events[13]. This can be achieved by changing the length or degree of cell depolarization, by altering the type or reducing the concentration of secretagogues (high K^+, Ba^{2+}, nicotine, α-latrotoxin and others) or by lowering the extracellular Ca^{2+} concentration.

Statistics

As the distributions of spike characteristics are often skewed[4,51] and may contain several subpopulations[26,52], statistical tests that assume normal distribution of data samples (ANOVA, *t* test among others) usually cannot be used. Moreover, as discussed in detail by Colliver and colleagues[53], analysis of individual parameter values pooled from several cells using nonparametric statistics or data resampling[54] may produce inconsistent results as pooled samples could be biased by recordings with a large number of events. Only in cases when the parameter distribution can be 'normalized' by taking a cube root or a logarithm of their values, does a nested (hierarchic) ANOVA test[55] yield a reliable outcome when comparing pooled spike characteristics from two cell populations[53]. For other spike characteristics, an alternative method should be used, which consists of calculating a mean parameter value for spikes recorded from one cell or release site and then comparing the samples of mean values from two groups of cells[53]. In case of heavily skewed distributions, the median or mode of values from individual recordings should be used as a more appropriate representation of population center[55]. This approach is particularly useful when comparing quantal sizes between experimental groups, as the distribution of average $Q^{1/3}$ or log(Q) values from several cells is normal[52,56], and parametric tests can be used. Similarly, parametric statistics can be used to analyze pooled PSF parameters that seem to follow lognormal distributions (Supplementary Fig. 2).

If a sample of spike characteristics is normally distributed, and the data are analyzed using parametric tests, the presence of occasional outliers may significantly bias the mean of the population. The outliers can be easily detected using normal probability plots, in which a Gaussian distribution of the data is represented by a straight line, and outliers are seen as datapoints that do not follow this line on the lower and upper sides of the graph[55]. These values are usually 2.5–3 standard deviations from the sample's mean and represent less than 1% of the population[35]. The presence of extreme values is less of a concern if nonparametric tests are used[55]. Finally, because recordings having different numbers of spikes have the same statistical 'weight', only cells that produce substantial number of release events, usually more that 10–20, are included in the analysis[53].

CONCLUSIONS

Amperometric recordings have vastly influenced the contemporary view of secretory neurotransmission by providing valuable information about the fine kinetics of transmitter release during vesicular exocytosis. The purpose of this review is to give practical guidelines for a nonspecialist who is interested in amperometric data acquisition and interpretation with the focus on the methodology of analysis of individual quanta events. We have paid particular attention to spike characteristics that can be derived or interpreted differently, as understanding these differences should help to standardize representation and comparison of data between various sources.

We incorporated the procedures that have been the most reliable in our experience into an open-source program written in Igor Pro that is available online (http://cumc.columbia.edu/dept/neurology/sulzer/download.html). Although several steps during the analysis are user-dependent (data filtering, using the cutoffs and others.), the majority of algorithms that identify the spikes and calculate their shape characteristics are independent of sampling rate and signal frequency, and have provided consistent results on amperometric traces from neurons (spikes are microseconds in duration), chromaffin cells (milliseconds) and even HPLC recordings (seconds).

Note: Supplementary information is available on the Nature Methods website.

ACKNOWLEDGMENTS

We thank M. Lindau, R. Staal and Y. Schmitz for critique of the manuscript and J.B. Sørensen, R. Borges and other participants of 12th International Symposium on Chromaffin Cell Biology for helpful discussion. Supported by Parkinson's Disease Foundation, Picower Foundation and National Institute of Drug Abuse grant 07418.

COMPETING INTERESTS STATEMENT

The authors declare that they have no competing financial interests.

Published online at http://www.nature.com/naturemethods/

1. Kissinger, P.T., Hart, J.B. & Adams, R.N. Voltammetry in brain tissue-a new neurophysiological measurement. *Brain Res.* **55**, 209–213 (1973).
2. Gonon, F. *et al. In vivo* continuous electrochemical determination of dopamine release in rat neostriatum. *C.R. Acad. Sci. Hebd. Seances. Acad. Sci. D* **286**, 1203–1206 (1978).
3. Leszczyszyn, D.J. *et al.* Nicotinic receptor–mediated catecholamine secretion

from individual chromaffin cells. Chemical evidence for exocytosis. *J. Biol. Chem.* **265**, 14736–14737 (1990).
4. Wightman, R.M. *et al.* Temporally resolved catecholamine spikes correspond to single vesicle release from individual chromaffin cells. *Proc. Natl. Acad. Sci. USA* **88**, 10754–10758 (1991).
5. Chen, T.K., Luo, G. & Ewing, A.G. Amperometric monitoring of stimulated catecholamine release from rat pheochromocytoma (PC12) cells at the zeptomole level. *Anal. Chem.* **66**, 3031–3035 (1994).
6. Pothos, E., Davila, V. & Sulzer, D. Presynaptic recording of quanta from midbrain dopamine neurons and modulation of the quantal size. *J. Neurosci.* **18**, 4106–4118 (1998).
7. Zhou, Z. & Misler, S. Amperometric detection of stimulus induced quantal release of catecholamines from cultured superior cervical ganglion neurons. *Proc. Natl. Acad. Sci. USA* **92**, 6938–6942 (1995).
8. Chen, G. & Ewing, A.G. Multiple classes of catecholamine vesicles observed during exocytosis from the *Planorbis* cell body. *Brain Res.* **701**, 167–174 (1995).
9. Alvarez de Toledo, G., Fernandez-Chacon, R. & Fernandez, J.M. Release of secretory products during transient vesicle fusion. *Nature* **363**, 554–558 (1993).
10. Bruns, D. & Jahn, R. Real-time measurement of transmitter release from single synaptic vesicles. *Nature* **377**, 62–65 (1995).
11. Huang, L., Shen, H., Atkinson, M.A. & Kennedy, R.T. Detection of exocytosis at individual pancreatic beta cells by amperometry at a chemically modified microelectrode. *Proc. Natl. Acad. Sci. USA* **92**, 9608–9612 (1995).
12. Paras, C.D. & Kennedy, R.T. Electrochemical detection of exocytosis at single rat melanotrophs. *Anal. Chem.* **67**, 3633–3637 (1995).
13. Chow, R.H. & von Ruden, L. Electrochemical detection of secretion from single cells. in *Single-channel recording* (eds. Sakmann, B. & Neher, E.) 245–276 (Plenum Press, New York, 1995).
14. Bruns, D. Detection of transmitter release with carbon fiber electrodes. *Methods* **33**, 312–321 (2004).
15. Dernick G. *et al.* Patch amperometry: high-resolution measurements of single-vesicle fusion and release *Nat. Methods* **2**, 699–708 (2005).
16. Rettig, J. & Neher, E. Emerging roles of presynaptic proteins in Ca^{2+}-triggered exocytosis. *Science* **298**, 781–785 (2002).
17. Jahn, R., Lang, T. & Sudhof, T.C. Membrane fusion. *Cell* ***112***, 519–533 (2003).
18. Burgoyne, R.D. & Morgan, A. Secretory granule exocytosis. *Physiol. Rev.* **83**, 581–632 (2003).
19. Chow, R.H., Von Rueden, L. & Neher, E. Delay in vesicle fusion revealed by electrochemical monitoring of single secretory events in adrenal chromaffin cells. *Nature* **356**, 60–63 (1992).
20. Zhou, Z., Misler, S. & Chow, R.H. Rapid fluctuations in transmitter release from single vesicles in bovine adrenal chromaffin cells. *Biophys. J.* **70**, 1543–1552 (1996).
21. Lindau, M. & Alvarez de Toledo, G. The fusion pore. *Biochim. Biophys. Acta* **1641**, 167–173 (2003).
22. Albillos, A. *et al.* The exocytic event in chromaffin cells revealed by patch amperometry. *Nature* **389**, 509–512 (1997).
23. Wightman, R.M., Troyer, K.P., Mundorf, M.L. & Catahan, R. The association of vesicular contents and its effects on release. *Ann. NY Acad. Sci.* **971**, 620–626 (2002).
24. Rahamimoff, R. & Fernandez, J.M. Pre- and postfusion regulation of transmitter release. *Neuron* **18**, 17–27 (1997).
25. Sombers, L.A. *et al.* The effects of vesicular volume on secretion through the fusion pore in exocytotic release from PC12 cells. *J. Neurosci.* **24**, 303–309 (2004).
26. Amatore, C. *et al.* Correlation between vesicle quantal size and fusion pore release in chromaffin cell exocytosis. *Biophys. J.* **88**, 4411–4420 (2005).
27. Curran, M.J. & Brodwick, M.S. Ionic control of the size of the vesicle matrix of beige mouse mast cells. *J. Gen. Physiol.* **98**, 771–790 (1991).
28. Marszalek, P.E., Farrell, B., Verdugo, P. & Fernandez, J.M. Kinetics of release of serotonin from isolated secretory granules. II. Ion exchange determines the diffusivity of serotonin. *Biophys. J.* **73**, 1169–1183 (1997).
29. Borges, R., Travis, E.R., Hochstetler, S.E. & Wightman, R.M. Effects of external osmotic pressure on vesicular secretion from bovine adrenal medullary cells. *J. Biol. Chem.* **272**, 8325–8331 (1997).
30. Amatore, C., Bouret, Y., Travis, E.R. & Wightman, R.M. Interplay between membrane dynamics, diffusion and swelling pressure governs individual vesicular exocytotic events during release of adrenaline by chromaffin cells. *Biochimie* **82**, 481–496 (2000).
31. Ales, E. *et al.* High calcium concentrations shift the mode of exocytosis to the kiss-and-run mechanism. *Nat. Cell Biol.* **1**, 40–44 (1999).
32. Henkel, A.W. & Almers, W. Fast steps in exocytosis and endocytosis studied by capacitance measurements in endocrine cells. *Curr. Opin. Neurobiol.* **6**, 350–357 (1996).
33. Palfrey, H.C. & Artalejo, C.R. Vesicle recycling revisited: rapid endocytosis may be the first step. *Neuroscience* **83**, 969–989 (1998).
34. Tabares, L., Lindau, M. & Alvarez de Toledo, G. Relationship between fusion pore opening and release during mast cell exocytosis studied with patch amperometry. *Biochem. Soc. Trans.* **31**, 837–841 (2003).
35. Sulzer, D. & Pothos, E.N. Presynaptic mechanisms that regulate quantal size. *Rev. Neurosci.* **11**, 159–212 (2000).
36. Staal, R.G., Mosharov, E.V. & Sulzer, D. Dopamine neurons release transmitter via a flickering fusion pore. *Nat. Neurosci.* **7**, 341–346 (2004).
37. Berg, H.C. Diffusion: macroscopic theory. in *Random Walks in Biology* (ed. Berg, H.C.) 17–36 (Princeton University Press, Princeton, NJ, 1983).
38. Schroeder, T.J. *et al.* Zones of exocytotic release on bovine adrenal medullary cells in culture. *J. Biol. Chem.* **269**, 17215–17220 (1994).
39. Travis, E.R. & Wightman, R.M. Spatio-temporal resolution of exocytosis from individual cells. *Annu. Rev. Biophys. Biomol. Struct.* **27**, 77–103 (1998).
40. Schroeder, T.J. *et al.* Temporally resolved, independent stages of individual exocytotic secretion events. *Biophys. J.* **70**, 1061–1068 (1996).
41. Wang, C.T. *et al.* Synaptotagmin modulation of fusion pore kinetics in regulated exocytosis of dense-core vesicles. *Science* **294**, 1111–1115 (2001).
42. Heinemann, S.H. Guide to data acquisition and analysis. in *Single-Channel Recording* (eds. Sakmann, B. & Neher, E.) 53–91 (Plenum Press, New York, 1995).
43. Schroeder, T.J. *et al.* Analysis of diffusional broadening of vesicular packets of catecholamines released from biological cells during exocytosis. *Anal. Chem.* **64**, 3077–3083 (1992).
44. Xu, T., Binz, T., Niemann, H. & Neher, E. Multiple kinetic components of exocytosis distinguished by neurotoxin sensitivity. *Nat. Neurosci.* ***1***, 192–200 (1998).
45. Segura, F. *et al.* Automatic analysis for amperometrical recordings of exocytosis. *J. Neurosci. Methods* **103**, 151–156 (2000).
46. Jankowski, J.A., Schroeder, T.J., Ciolkowski, E.L. & Wightman, R.M. Temporal characteristics of quantal secretion of catecholamines from adrenal medullary cells. *J. Biol. Chem.* **268**, 14694–14700 (1993).
47. Jankowski, J.A., Finnegan, J.M. & Wightman, R.M. Extracellular ionic composition alters kinetics of vesicular release of catecholamines and quantal size during exocytosis at adrenal medullary cells. *J. Neurochem.* **63**, 1739–1747 (1994).
48. Sorensen, J.B. *et al.* Differential control of the releasable vesicle pools by SNAP-25 splice variants and SNAP-23. *Cell* **114**, 75–86 (2003).
49. Alvarez de Toledo, G. & Fernandez, J.M. Compound versus multigranular exocytosis in peritoneal mast cells. *J. Gen. Physiol.* **95**, 397–409 (1990).
50. Hafez, I., Stolpe, A. & Lindau, M. Compound exocytosis and cumulative fusion in eosinophils. *J. Biol. Chem.* **278**, 44921–44928 (2003).
51. Glavinovic, M.I., Vitale, M.L. & Trifaro, J.M. Comparison of vesicular volume and quantal size in bovine chromaffin cells. *Neuroscience* **85**, 957–968 (1998).
52. Tang, K.S., Tse, A. & Tse, F.W. Differential regulation of multiple populations of granules in rat adrenal chromaffin cells by culture duration and cyclic AMP. *J. Neurochem.* **92**, 1126–1139 (2005).
53. Colliver, T. *et al.* Quantitative and statistical analysis of the shape of amperometric spikes recorded from two populations of cells. *J. Neurochem.* **74**, 1086–1097 (2000).
54. Van der Kloot, W. Statistics for studying quanta at synapses: resampling and confidence limits on histograms. *J. Neurosci. Methods* **65**, 151–155 (1996).
55. Ott, R.L. & Longnecker, M. *An Introduction to Statistical Methods and Data Analysis* (Duxbury Press, Belmont, California, 2001).
56. Pothos, E. *et al.* D2-like dopamine autoreceptor activation reduces quantal size in PC12 cells. *J. Neurosci.* **18**, 5575–5585 (1998).
57. Baur, J.E. *et al.* Fast-scan voltammetry of biogenic amines. *Anal. Chem.* **60**, 1268–1272 (1988).
58. Colquhoun, D. & Sigworth, F.J. Fitting and statistical analysis of single-channel records. in *Single-Channel Recording* (eds. Sakmann, B. & Neher, E.) 483–587 (Plenum Press, New York, 1995).
59. Gomez, J.F. *et al.* New approaches for analysis of amperometrical recordings. *Ann. NY Acad. Sci.* **971**, 647–654 (2002).